Bound states in the continuum for an array of quantum emitters

Paolo Facchi,[1,2] Davide Lonigro,[1,2] Saverio Pascazio,[1,2,3] Francesco V. Pepe [2] and Domenico Pomarico[1,2]

[1]*Dipartimento di Fisica and MECENAS, Università di Bari, I-70126 Bari, Italy*
[2]*INFN, Sezione di Bari, I-70126 Bari, Italy*
[3]*Istituto Nazionale di Ottica (INO-CNR), I-50125 Firenze, Italy*

We study the bound states in the continuum for a system of n two-level quantum emitters, coupled with a one-dimensional photon field, when a single excitation is shared among the different components of the system. The emitters are equally spaced at fixed positions. We first consider the approximation of distant emitters and exhibit degenerate eigenspaces of bound states corresponding to resonant discrete values of the energy. We then consider the full form of the eigenvalue equation, in which the effects of the finite spacing and the field dispersion relation become relevant, yielding significant nonperturbative effects that can lift some degeneracies. We explicitly solve the cases $n = 3$ and $n = 4$ emitters.

I. INTRODUCTION

The physics of effectively one-dimensional (1D) systems is recently attracting increasing attention, thanks to the unprecedented possibilities offered by modern quantum technologies [1]. A number of interesting and versatile experimental platforms are available nowadays to implement an efficient dimensional reduction and enable photon propagation in 1D. These schemes differ in scope and make use of diverse physical systems, such as optical fibers [2,3], cold atoms [4–6], superconducting qubits [7–13], photonic crystals [14–18], and quantum dots in photonic nanowires [19,20], the list being far from exhaustive. Light propagation in these systems is characterized by different energy dispersion relations and interaction form factors, yielding drastically dimension-dependent features that heavily affect dynamics, decay, and propagation [21,22].

Although the physics of *single* quantum emitters in waveguides is well understood [4,12,23–26], novel phenomena arise when *two* [27–39] or *more* [17,18,21,23,25,40–57] emitters are present, since the dynamics is influenced by photon-mediated quantum correlations. In this and similar contexts, sub- and super-radiant states often emerge. However, while standard (Dicke) super-radiance effects occur at light wavelengths much larger than typical interatomic distances [58–61], considering wavelengths comparable to the interatomic distance brings to light a number of interesting quantum resonance effects [62].

In this article, we will apply the resolvent formalism [63] to study the existence of single-excitation bound states in the continuum in a system of n quantum emitters. In these states, the excitation is shared in a stable way between the emitters and the field, even though the energy would be sufficient to yield photon propagation. The case of $n = 2$ emitters has already been considered in both the one- and two-excitation sectors [29,64]. Here we extend the results to general n, under the assumption of large interatomic spacing compared to the inverse infrared cutoff of the waveguide mode. We will then consider how the corrections to such approximation crucially

affect the physical picture of the system, by explicitly analyzing the cases of $n = 3$ and $n = 4$ emitters, and briefly reviewing the case $n = 2$.

The paper is structured as follows. In Sec. II we introduce the physical system, the interaction Hamiltonian, and the relevant parameters. In Sec. III we outline the general properties of bound states in the continuum. In Sec. IV we analyze and discuss the eigenvalues in the continuum and the corresponding eigenspaces. In Sec. V we comment on the existence of nonperturbative eigenstates that emerge when the interatomic spacing is smaller than a critical value, depending on the number n. In Sec. VI we summarize our main results.

II. PHYSICAL SYSTEM AND HAMILTONIAN

We shall consider a system of n two-level emitters, equally spaced at a distance d and characterized by the same excitation energy ε. Henceforth, we shall occasionally refer to the emitters as "atoms." The ground and excited state of each emitter will be denoted by $|g_j\rangle$ and $|e_j\rangle$, respectively, with $j = 1, \ldots, n$. The emitter array is coupled to a structured one-dimensional photon continuum (e.g., a waveguide mode), characterized by a dispersion relation $\omega(k) \geqslant 0$, with $k \in \mathbb{R}$, and represented by the canonical field operators $b(k)$ and $b^\dagger(k)$, satisfying $[b(k), b^\dagger(k')] = \delta(k - k')$. In absence of interactions, the Hamiltonian of the system reads

$$H_0 = \varepsilon \sum_{j=1}^{n} |e_j\rangle\langle e_j| + \int dk\, \omega(k) b^\dagger(k) b(k). \qquad (1)$$

When the total Hamiltonian $H = H_0 + H_{\text{int}}$ is considered, the interacting dynamics generally does not preserve the total number of excitations,

$$\mathcal{N} = \sum_{j=1}^{n} |e_j\rangle\langle e_j| + \int dk\, b^\dagger(k) b(k), \qquad (2)$$
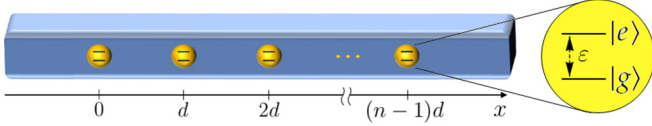
FIG. 1. The system: n two-level emitters placed at a relative distance d and characterized by excitation energy ε.

unless a rotating-wave approximation is applied. In this case, the interaction Hamiltonian reads

$$H_{\text{int}} = \sum_{j=1}^{n} \int dk [F(k) e^{i(j-1)kd} |e_j\rangle\langle g_j| b(k) + \text{H.c.}], \quad (3)$$

where $F(k) e^{i(j-1)kd}$ is the form factor describing the strength of the coupling of the jth emitter standing at $x = (j-1)d$ with a photon of momentum k, and H can be diagonalized in orthogonal sectors characterized by a fixed eigenvalue of $\mathcal{N}$. The system is sketched in Fig. 1.

The zero-excitation sector, $\mathcal{N} = 0$, is spanned by the ground state of H_0, $|G^{(n)}\rangle \otimes |\text{vac}\rangle$, with

$$|G^{(n)}\rangle = \bigotimes_{j=1}^{n} |g_j\rangle \quad (4)$$

and $|\text{vac}\rangle$ being the vacuum photon state and $b(k)|\text{vac}\rangle = 0$ for all k's.

In this article, we will focus on the search of bound states in the one-excitation sector, $\mathcal{N} = 1$, whose vectors have the form

$$|\Psi_1\rangle = \sum_{j=1}^{n} a_j |E_j^{(n)}\rangle \otimes |\text{vac}\rangle + |G^{(n)}\rangle \otimes \int dk\, \xi(k) b^\dagger(k)|\text{vac}\rangle, \quad (5)$$

with

$$|E_j^{(n)}\rangle = |g_1\rangle \otimes \cdots \otimes |g_{j-1}\rangle \otimes |e_j\rangle \otimes |g_{j+1}\rangle \otimes \cdots \otimes |g_n\rangle. \quad (6)$$

In particular, we will consider a photon continuum with a massive dispersion relation

$$\omega(k) = \sqrt{k^2 + m^2}, \quad (7)$$

and a form factor

$$F(k) = \sqrt{\frac{\gamma}{2\pi\,\omega(k)}}, \quad (8)$$

determined by the $\boldsymbol{p} \cdot \boldsymbol{A}$ interaction of QED [63], with γ a coupling constant with the dimensions of squared energy.

The Hamiltonian $H = H_0 + H_{\text{int}}$, defined by the dispersion relation (7) and by the form factor (8), depends on the four parameters ε, m, d, and γ, all with physical dimension.

III. BOUND STATES IN THE CONTINUUM

We are interested in bound states in the continuum of the one-excitation sector, that is, eigenstates with energy $E > m$. By considering the Hamiltonian $H = H_0 + H_{\text{int}}$, defined by (1) and (3), and the expansion of the state vectors (5), the

eigenvalue equation in the one-excitation sector reads

$$(\varepsilon - E)a_j = -\int dk\, e^{-i(j-1)kd} F(k)^* \xi(k)$$

$$[\omega(k) - E]\xi(k) = -\sum_{\ell=1}^{n} a_\ell\, e^{i(\ell-1)kd} F(k). \quad (9)$$

From the second equation,

$$\xi(k) = -\sum_{\ell=1}^{n} a_\ell\, e^{i(\ell-1)kd} \frac{F(k)}{\omega(k) - E}, \quad (10)$$

one infers that, since $\xi(k)$ must be normalizable for a bound state, the vanishing of the denominator, occurring when $\omega(k) = E$, i.e., at $k = \pm\bar{k}$, with

$$\bar{k}(E) = \sqrt{E^2 - m^2}, \quad (11)$$

for $E > m$, must be compensated by the vanishing of the numerator at the same points. Therefore, the atomic excitation amplitudes and the energy eigenvalue of bound states in the continuum necessarily satisfy the constraint

$$\sum_{\ell=1}^{n} a_\ell e^{\pm i(\ell-1)\bar{k}d} = 0. \quad (12)$$

By using the expression (10), one obtains the relation

$$(\varepsilon - E)a_j = \int dk \sum_{\ell=1}^{n} \frac{a_\ell\, e^{i(\ell-j)kd}\, |F(k)|^2}{\omega(k) - E}, \quad (13)$$

involving only the atomic excitation amplitudes and the eigenvalue E. Equation (13) can be expressed in the compact form

$$G^{-1}(E)\boldsymbol{a} = \boldsymbol{0}, \quad (14)$$

with $\boldsymbol{a} = (a_1, a_2, \ldots, a_n)^T$ and G^{-1} the inverse propagator matrix in the single-atomic-excitation subspace, generally defined for a complex energy z by

$$G^{-1}(z) = (\varepsilon - z)\mathbb{1} - \Sigma(z), \quad (15)$$

where the self-energy matrix Σ has elements

$$\Sigma_{j\ell}(z) = \int dk \frac{|F(k)|^2}{\omega(k) - z} e^{-i(j-\ell)kd}. \quad (16)$$

The self-energy and the inverse propagator are well defined for nonreal arguments and have a discontinuity across the continuum spectrum $z \in [m, \infty)$, where generally

$$\Sigma(E + i0) - \Sigma(E - i0) \neq 0, \qquad E \in [m, \infty), \quad (17)$$

with $\Sigma(E \pm i0) = \lim_{\delta\downarrow 0} \Sigma(E \pm i\delta)$.

Therefore, the equality of the upper and lower boundary value is a necessary condition for (14) to be well defined and, *a fortiori*, for E to be an eigenvalue. Finally, notice that Eq. (14) always admits a trivial solution, which correspond, due to (10), to the null vector. If $G^{-1}(E)$ is well defined, then the equation

$$\det G^{-1}(E) = 0 \quad (18)$$

provides a necessary and sufficient condition for E to be an eigenvalue with a nontrivial solution $\boldsymbol{a} \neq \boldsymbol{0}$, providing the atomic excitation amplitudes of the corresponding eigenstate.
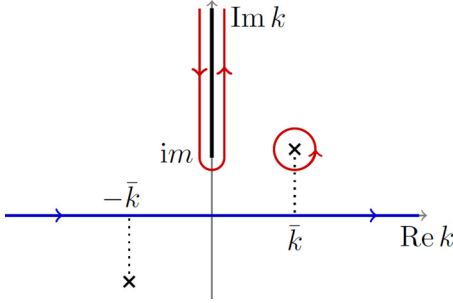
FIG. 2. Integration contour in the complex k plane for the computation of the self-energy matrix $\Sigma(z)$. The integral on the (blue) contour along the real axis is evaluated as the sum of the integrals on the circle enclosing $\bar{k}$ (pole contribution) and along the cut $(im, i\infty)$ (cut contribution).

The integrals that define the elements of the self-energy in (16) can be evaluated for $z = E \pm i0$ with $E > m$ by analytic continuation in the complex k plane, yielding

$$\Sigma_{jl}(E \pm i0) = \frac{\pm i\gamma}{\bar{k}(E)}[e^{\pm i|j-l|\bar{k}(E)d} \pm i\, b_{|j-l|}(E)], \qquad (19)$$

where the first term derives from integration around one of the poles at $k = \pm\bar{k}$ and the second one,

$$b_j(E) = \frac{\bar{k}(E)}{\pi} \int_m^\infty d\kappa \frac{e^{-j\kappa d}}{\sqrt{\kappa^2 - m^2}} \frac{E}{E^2 + \kappa^2 - m^2}, \qquad (20)$$

from integration around one of the branch cuts, $(im, i\infty)$ or $(-i\infty, im)$, of the analytic continuation in the complex k plane. The original and modified integration contours are shown in Fig. 2. Notice that the functions b_j are real for $E > m$.

In the case $j = 0$, the integral can be evaluated analytically and yields

$$b_0(E) = -\frac{1}{\pi} \ln\left(\frac{E - \sqrt{E^2 - m^2}}{m}\right). \qquad (21)$$

In the general case, the cut contribution must be evaluated numerically. However, a relevant property follows from the definition (20),

$$\frac{|b_j(E)|}{|b_0(E)|} \leqslant \exp(-jmd) \quad \text{for } E > m, \qquad (22)$$

implying that, for $md \gg 1$, the terms $b_{j>0}$ can be neglected as a first approximation.

In the following, we will show that, interestingly, the inclusion of such terms in the analysis on one hand entails selection rules that remove the degeneracy of bound states in the continuum and, on the other hand, displaces by orders $O(e^{-md})$ the energies, resonance distances, and amplitudes that satisfy the constraint in Eq. (12).

The photon eigenfunction (10) in the position representation reads

$$\xi(x) = -\int dk \frac{F(k)}{\omega(k) - E} \sum_{\ell=1}^n a_\ell e^{-ik[x-(\ell-1)d]}$$

$$= \sum_{\ell=1}^n a_\ell \xi_1(x - (\ell-1)d) \qquad (23)$$

with

$$\xi_1(x) = -\fint dk \frac{F(k)}{\omega(k) - E} e^{-ikx}$$

$$= \frac{\sqrt{\gamma E}}{\bar{k}}[\sin(\bar{k}|x|) - \eta(x)], \qquad (24)$$

where $\fint$ denotes integration with the principal value prescription and

$$\eta(x) = \frac{1}{2\pi} \frac{\bar{k}}{\sqrt{2E}} \int_m^\infty d\kappa \frac{e^{-\kappa|x|}}{\sqrt[4]{\kappa^2 - m^2}} \frac{\sqrt{\kappa^2 - m^2} - E}{E^2 + \kappa^2 - m^2} \qquad (25)$$

is the $O(e^{-mx})$ cut contribution. Notice that the principal value prescription $\fint$ is required in the definition of ξ_1 for $E > m$, while the integral in $\xi(x)$ is regularized by the constraint (12).

IV. EIGENVALUES AND EIGENSTATES

A. Block-diagonal representation of the propagator

Given the form (14) of the eigenvalue equation for the atomic amplitude vector $\boldsymbol{a}$ and the dependence of the propagator on the interatomic distance d and the transition energy ε, it is convenient to introduce the matrix $A_n(\theta, \chi, \boldsymbol{b})$, depending on $n + 1$ real parameters, $\theta, \chi \in \mathbb{R}$, $\boldsymbol{b} \in \mathbb{R}^{n-1}$, and defined as

$$[A_n(\theta, \chi, \boldsymbol{b})]_{j\ell} = \begin{cases} 1 + i\chi, & \text{for } j = \ell \\ e^{i|j-\ell|\theta} + ib_{|j-\ell|}, & \text{for } j \neq \ell \end{cases}, \qquad (26)$$

with $j, \ell = 1, \ldots, n$, that is,

$$A_n(\theta, \chi, \boldsymbol{b}) = \begin{pmatrix} 1 + i\chi & e^{i\theta} + ib_1 & e^{i2\theta} + ib_2 & \ldots \\ e^{i\theta} + ib_1 & 1 + i\chi & e^{i\theta} + ib_1 & \ldots \\ e^{i2\theta} + ib_2 & e^{i\theta} + ib_1 & 1 + i\chi & \ldots \\ e^{i3\theta} + ib_3 & e^{i2\theta} + ib_2 & e^{i\theta} + ib_1 & \ldots \\ \vdots & \vdots & \vdots & \ddots \end{pmatrix}. \qquad (27)$$

The inverse propagator reads

$$G^{-1}(E) = -\frac{i\gamma}{\bar{k}(E)} A_n(\theta(E), \chi(E), \boldsymbol{b}(E)), \qquad (28)$$

with

$$\theta(E) = \bar{k}(E)d, \qquad (29)$$

$$\chi(E) = \frac{\varepsilon - E}{\gamma}\bar{k}(E) + b_0(E), \qquad (30)$$

and $\bar{k}(E)$, $b_{j>0}(E)$, and $b_0(E)$ as defined in (11), (20), and (21), respectively.

The matrix A_n can be recast in block-diagonal form by exploiting the invariance of the Hamiltonian with respect to spatial reflections at the midpoint $x = (n - 1)d/2$, transforming the local-excitation basis $|E_j^{(n)}\rangle$ in (6) by the unitary

transformation

$$U_n \left| E_j^{(n)} \right\rangle = \begin{cases} \dfrac{\left| E_j^{(n)} \right\rangle - \left| E_{n-j}^{(n)} \right\rangle}{\sqrt{2}} & \text{for } j \leqslant \frac{n}{2} \\[2mm] \left| E_j^{(n)} \right\rangle & \text{for } j = \frac{n+1}{2} \\[2mm] \dfrac{\left| E_j^{(n)} \right\rangle + \left| E_{n-j}^{(n)} \right\rangle}{\sqrt{2}} & \text{for } j \geqslant \frac{n}{2} + 1 \end{cases} . \tag{31}$$

The action of such a transformation, which is also real and symmetric, on the components in the local basis can be expressed for even $n = 2h$ and odd $n = 2h + 1$ in terms of the $h \times h$ identity matrix $\mathbb{1}_h$ and the "exchange" matrix J_h (i.e., the matrix with ones on the counterdiagonal as the only nonvanishing elements) as

$$U_n = \frac{1}{\sqrt{2}} \begin{pmatrix} \mathbb{1}_h & -J_h \\ J_h & \mathbb{1}_h \end{pmatrix} \tag{32}$$

and

$$U_n = \frac{1}{\sqrt{2}} \begin{pmatrix} \mathbb{1}_h & 0 & -J_h \\ 0 & \sqrt{2} & 0 \\ J_h & 0 & \mathbb{1}_h \end{pmatrix}, \tag{33}$$

respectively. The transformation U_n generalizes the change from the local basis to the Bell basis for $n = 2$ emitters [29].

In the new representation, the self-energy and the propagator turn out to be block diagonal:

$$U_n A_n U_n^\dagger = A_n^- \oplus A_n^+, \tag{34}$$

where $A_n^-(\theta, \chi, \boldsymbol{b})$ is the $\lfloor n/2 \rfloor \times \lfloor n/2 \rfloor$ matrix acting on the antisymmetric amplitude vectors of the emitters, with

$$a_j = -a_{n+1-j}, \quad j = 1, \ldots, n, \tag{35}$$

and $A_n^+(\theta, \chi, \boldsymbol{b})$ is the $\lceil n/2 \rceil \times \lceil n/2 \rceil$ matrix acting on the symmetric amplitude vectors, with

$$a_j = a_{n+1-j}, \quad j = 1, \ldots, n. \tag{36}$$

Therefore, the eigenvalue equation (14) can be reduced to the quest for nontrivial solutions of the two decoupled linear systems

$$A_n^\pm(\theta(E), \chi(E), \boldsymbol{b}(E)) \boldsymbol{a}^\pm = 0. \tag{37}$$

Eigenvectors with no reflection symmetry are allowed only if the same energy E is an eigenvalue for both systems (37) for the same set of parameters ε, m, d, and γ. Examples of eigenstates with definite symmetry, whose relevance will be discussed in the following, are shown in Fig. 3.

Throughout this section, we will first analyze bound states by neglecting $O(e^{-md})$ terms in the self-energy and then discuss the consequences of including all the $b_{j>0}$ terms in the cases $n = 2, 3, 4$.

B. Large spacing approximation

When md is large, the terms b_j, with $j > 0$, in the self-energy are exponentially suppressed and will be neglected as a first approximation, namely

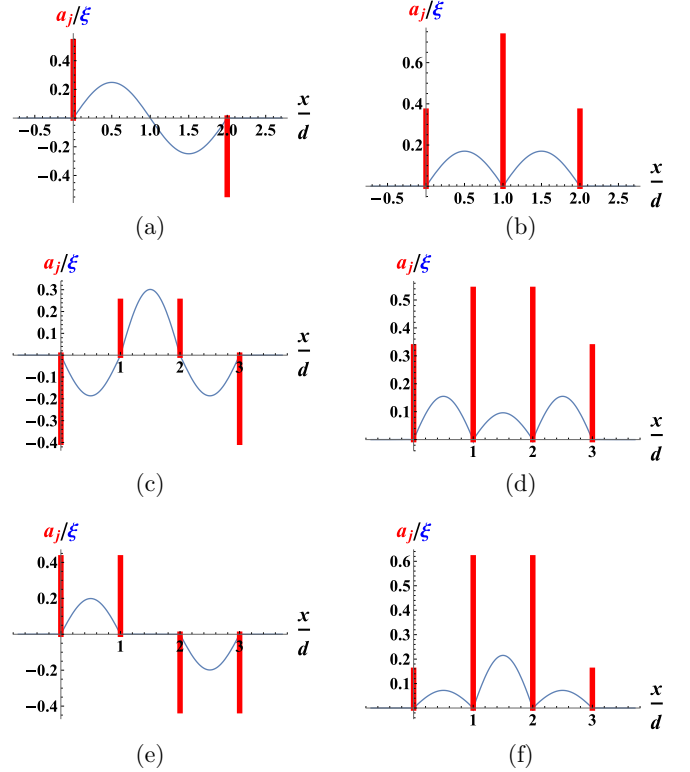$$\boldsymbol{b} = \boldsymbol{0}. \tag{38}$$

FIG. 3. Atomic excitation amplitudes a_j, with $1 \leqslant j \leqslant n$, represented as (red) bars localized at the emitter positions, and field wave functions $\xi(x)$, represented as solid (blue) lines, for different bound states in the continuum of a system of $n = 3$ [(a) and (b)] and $n = 4$ [(c)–(f)] emitters with $md = 7$ and $\gamma/m^2 = 10^{-2}$. In panel (a), $a_1 = -a_3$ and $a_2 = 0$; in panel (b), $a_1 = a_3$ and $a_2/a_1 \simeq 2$; in panel (c), $a_1 = a_4$, $a_2 = a_3$ and $a_1/a_2 \simeq -(1 + \sqrt{5})/2$; in panel (d), $a_1 = a_4$, $a_2 = a_3$ and $a_1/a_2 \simeq (\sqrt{5} - 1)/2$; in panel (e), $a_1 = a_2$, $a_3 = a_4$ and $a_2 = -a_3$; in panel (f), $a_1 = a_4$, $a_2 = a_3$ and $a_1/a_2 \simeq 0.25$.

Both matrices $A_n^\pm(\theta, \chi, \boldsymbol{0})$ are singular if and only if

$$\theta = \nu\pi \quad (\nu \in \mathbb{N}), \quad \text{and} \quad \chi = 0. \tag{39}$$

The former condition,

$$\bar{k} = \frac{\nu\pi}{d}, \tag{40}$$

selects the possible eigenvalues in terms of the spacing d,

$$E = E_\nu(d) = \sqrt{\frac{\nu^2\pi^2}{d^2} + m^2}, \tag{41}$$

which will be called *resonant energies* in the following. Notice that (40) implies that the emitters should be at a distance d which is an exact multiple of half wavelengths of the trapped photon $\bar{\lambda} = 2\pi/\bar{k}$, that is, $d = \nu\bar{\lambda}/2$.

The second condition in (39),

$$\begin{aligned} \varepsilon &= E_\nu(d) - \frac{\gamma d}{\nu\pi} b_0[E_\nu(d)] \\ &= E_\nu(d) + \frac{\gamma d}{\nu\pi} \ln\left[\frac{E_\nu(d)}{m} - \frac{\nu\pi}{md}\right], \end{aligned} \tag{42}$$

provides a constraint involving the excitation energy, the spacing, and the order ν of the resonance. Equation (42) defines a

discrete family of curves in the (ε, d) plane, identifying the values ε for which a bound state in the continuum exists.

The emitter configurations associated with the eigenvalues (41) satisfy the constraint (12), which yields two different conditions according to the parity of the resonance. For even ν, for all the eigenvectors, the atomic excitation amplitudes must sum to zero,

$$\sum_{j=1}^{n} a_j = 0; \tag{43}$$

while for odd ν one obtains

$$\sum_{j=1}^{n} (-1)^j a_j = 0. \tag{44}$$

Hence, each eigenvalue $E_\nu(d)$ is characterized by an $(n-1)$-fold degeneracy. It is worth observing that, since both matrices $A_n^\pm$ are characterized by the same singularity conditions at this level of approximation, the same eigenvalue can occur in both the symmetric and antisymmetric sector. In such cases, the bound states are not characterized by a well-defined symmetry.

The photon wave function associated with the eigenstates can be derived according to Eq. (23), considering $E = E_\nu(d)$. Neglecting the η contribution in (24), the single-emitter contribution to the field is given by the oscillating function

$$\xi_1(x) \propto \sin\left(\frac{\nu \pi |x|}{d}\right), \tag{45}$$

whose half-wavelength coincides with d/ν. The photon wave function in the same approximation thus reads

$$\xi(x) \propto \sum_{\ell=1}^{n} a_\ell \, \mathrm{sgn}[x - (\ell-1)d] \, \sin\left(\frac{\nu \pi x}{d}\right) \tag{46}$$

for even ν and

$$\xi(x) \propto \sum_{\ell=1}^{n} a_\ell \, (-1)^{\ell-1} \mathrm{sgn}[x - (\ell-1)d] \, \sin\left(\frac{\nu \pi x}{d}\right) \tag{47}$$

for odd ν. The field has nodes at the emitter positions $x = jd$ and in both cases, due to the conditions (43) and (44), respectively, it vanishes identically for $x < 0$ and $x > nd$ and is therefore confined inside the emitter array.

Finally, it is worth observing that all possible n-emitter eigenstates can be obtained as linear combinations of two-emitter eigenstates at different positions. However, we will show in the following that $O(e^{-md})$ effects, however small, remove this degeneracy, and imply selection rules related to the reflection symmetry of the atomic eigenstates.

C. Full form of the self-energy

The degeneracy obtained in the previous subsection by approximating the self-energy by setting $\boldsymbol{b} = \boldsymbol{0}$ is lifted by considering the terms b_j, with $j > 0$. We now discuss in detail this phenomenon. The effect of these terms can be summarized in the following points:

(i) At given d and $E_\nu(d)$, only one of the two matrices $A_n^\pm(\nu\pi, \chi[E_\nu(d)], \boldsymbol{b}[E_\nu(d)])$, namely the one for which

$$A_n^\pm(\nu\pi, 0, \boldsymbol{0}) = 0, \tag{48}$$

continues to be singular for some values of ε and γ. The matrix satisfying the property (48) is the antisymmetric one for odd n and the one with symmetry $(-1)^{\nu+1}$ for even n. Details on this general result are given in the Appendix.

(ii) The values of $\chi(E)$ [and hence of ε, through Eq. (42)] corresponding to the eigenstates with energy $E_\nu(d)$ will depend on the eigenstate. For any fixed ε, only one stable state with energy $E_\nu(d)$ can generally be found, with the orthogonal states becoming unstable (although possibly long lived).

(iii) If $A_n^\pm(\nu\pi, 0, \boldsymbol{0})$ does not satisfy condition (48), then $A_n^\pm(\nu\pi, \chi[E_\nu(d)], \boldsymbol{b}[E_\nu(d)])$ is in general no longer singular. However, the corresponding stable states do not entirely disappear but undergo a slight change in their amplitude and energy, which is now displaced with respect to $E_\nu(d)$. Such states must be studied numerically.

Here, we will explicitly examine these effects in the three cases of $n = 2, 3, 4$ emitters. Moreover, we shall focus on eigenstates connected by continuity to the resonant bound states discussed in the previous subsection and postpone to Sec. V the study of strong-coupling eigenstates, distant from the resonant values, and characterized by extremely high energies, $E/m \gtrsim 10^2$.

1. n = 2 emitters

With respect to the inclusion of the cut terms $\boldsymbol{b}$ in the self-energy, $n = 2$ represents an oversimplified case, since the linear systems $A_n^\pm(\theta, \chi, \boldsymbol{b})$ reduce to single equations, and the singularity conditions read

$$A_2^\pm(\theta, \chi, b_1) = 1 \pm e^{i\theta} + i(\chi \pm b_1) = 0, \tag{49}$$

corresponding to eigenstates in which the emitter excitation amplitudes exactly satisfy

$$a_2 = \pm a_1. \tag{50}$$

The peculiarity of $n = 2$ lies in the fact that the condition $\theta = \nu\pi$, with odd ν in the symmetric sector and even ν in the antisymmetric sector, still holds for both symmetries, yielding a resonant eigenenergy (41). The second condition in (39) is generalized to

$$\chi = (-1)^\nu b_1, \tag{51}$$

so that the emitter excitation energy is constrained by

$$\varepsilon = E_\nu(d) - \frac{\gamma d}{\nu\pi}\{b_0[E_\nu(d)] - (-1)^\nu b_1[E_\nu(d)]\}. \tag{52}$$

In this case, the inclusion of $b_1 = O(e^{-md})$ in the self-energy does not shift energies away from the resonant values and does not remove any degeneracy, since the symmetric and antisymmetric eigenstates already occurred for different ν's [29].

2. n = 3 emitters

For a system of three emitters, the eigenvalue equation breaks down into a single equation for the antisymmetric sector and a system of two equations for the symmetric sector. In the former case, the eigenvalues are determined by the solution of

$$A_3^-(\theta, \chi, \boldsymbol{b}) = 1 - e^{2i\theta} + i(\chi - b_2) = 0. \tag{53}$$

As in the $n = 2$ case, the real part of the above equation is sufficient to ensure that the resonance condition $\theta = \nu\pi$, here with any $\nu \in \mathbb{N}$, is still valid, and the corresponding energy must be resonant (41). The constraint on ε for the existence of an antisymmetric eigenstate, with the atomic excitation proportional to $(|E_3^{(1)}\rangle - |E_3^{(3)}\rangle)/\sqrt{2}$, is now determined by the equation

$$\chi = b_2, \qquad (54)$$

which yields

$$\varepsilon = E_\nu(d) - \frac{\gamma d}{\nu\pi}\{b_0[E_\nu(d)] - b_2[E_\nu(d)]\}. \qquad (55)$$

Instead, in the symmetric sector, where the eigenenergies are determined by the equation

$$
\begin{aligned}
0 &= \det A_3^+(\theta, \chi, \boldsymbol{b}) \\
&= \det \begin{bmatrix} 1 + i\chi & \sqrt{2}(e^{i\theta} + ib_1) \\ \sqrt{2}(e^{i\theta} + ib_1) & 1 + e^{2i\theta} + i(\chi + b_2) \end{bmatrix},
\end{aligned}
\qquad (56)
$$

one can easily check that there are no solutions for $\theta = \nu\pi$ with integer ν, as their existence would imply at least one of the conditions $b_2(E) = \pm 3\sqrt{b_1(E)^2 \pm 2b_1(E)}$. Actually, the energy of the symmetric bound state in the continuum

$$E = E_\nu(d) + (-1)^\nu \frac{\bar{k}[E_\nu(d)]}{d\, E_\nu(d)} b_1[E_\nu(d)] + O(e^{-2md}) \quad (57)$$

is shifted by an amount of $O(e^{-md})$ with respect to the resonant value $E_\nu(d)$, corresponding to a shift $\delta\theta \simeq (-1)^\nu b_1[E_\nu(d)]$ in the phase. The values of (ε, d) at which the symmetric bound states occur can now be derived from the condition

$$\chi(E) = 2(-1)^\nu b_1[E_\nu(d)] + O(e^{-2md}), \qquad (58)$$

with E given by (57). For the lowest-order resonances $\nu = 1$, one can observe that the energy of the symmetric state is shifted downward with respect to the value $E_1(d)$, that is exact for the antisymmetric state. This effect is evident in Fig. 4, in which the behavior of the eigenvalues corresponding to bound states in the continuum for both parity sector is represented in terms of d. The trajectories of the bound states are displayed in Fig. 5.

While the excitation amplitudes of antisymmetric bound states are constrained to the values

$$a_2 = 0, \quad a_3 = -a_1, \qquad (59)$$

the amplitudes of the symmetric states depend on the parameters and on the magnitude of the cut contributions. If the terms $b_{j>0}$ are neglected, then the symmetric bound state is characterized by

$$a_3 = a_1, \quad a_2 \simeq 2(-1)^{\nu+1}a_1, \qquad (60)$$

with the second value sensitive to $O(e^{-md})$ corrections when the b_j's are included. These states are represented in Figs. 3(a) and 3(b), for some values of the parameters d and γ. In the following section, we will find that bound states with different amplitudes, not connected by continuity to the ones described above, can emerge in the case $\varepsilon \gg m$, a regime in which, however, the validity of the one-dimensional approximation on which our model is based becomes questionable.
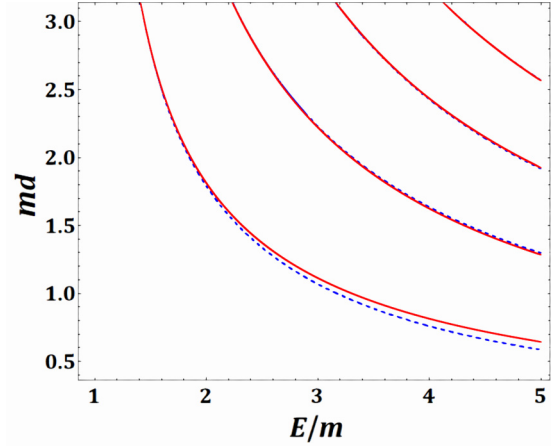

FIG. 4. Spectral lines in the (E, d) plane for a system of $n = 3$ equally spaced emitters. Solid (red) lines correspond to antisymmetric configurations, while dashed (blue) lines to symmetric ones. For larger values of the distance, the curves follow with excellent approximation the resonant values in Eq. (41). For $md \lesssim 2$, the difference between the eigenvalues of the lowest-energy symmetric and antisymmetric state becomes appreciable.

A relevant parameter that characterizes the features of bound states in the continuum is the total probability of atomic excitations,

$$p = \boldsymbol{a}^\dagger \boldsymbol{a} = 1 - \int dk |\xi(k)|^2, \qquad (61)$$

that "measures" how the single excitation is shared between the emitters and the field. In this case, the probabilities $p_\nu^{(3)\pm}$ for the symmetric $(+)$ and antisymmetric $(-)$ eigenstates read

$$p_\nu^{(3)+} \simeq \left[1 + \frac{2\gamma dE_\nu}{3(E_\nu^2 - m^2)} + \frac{\gamma}{\pi(E_\nu + m)}\right]^{-1}, \qquad (62)$$

$$p_\nu^{(3)-} \simeq \left[1 + \frac{2\gamma dE_\nu}{E_\nu^2 - m^2} + \frac{2\gamma}{\pi(E_\nu + m)}\right]^{-1}, \qquad (63)$$

up to order $O(e^{-md})$.

As in the case of $n = 2$ emitters [29], the emitter excitation decreases with coupling and distance and increases with energy. In Fig. 6 we show the probabilities for the symmetric and antisymmetric states with $\nu = 1$, computed from the approximate expressions (62) and (63) as a function of d and γ. In the whole parameter range, the approximate expressions provide, even for small md, a very good estimate of the exact values, which differ by less than 10^{-3} in the symmetric case and less than 2.5×10^{-2} in the antisymmetric case.

3. $n = 4$ emitters

For a system made up of $n = 4$ emitters, the eigenvalues in both symmetry sectors are determined by the singularity conditions of the 2×2 matrices

$$A_4^\pm = \begin{bmatrix} 1 \pm e^{i\theta} + i(\chi \pm b_1) & e^{i\theta} \pm e^{2i\theta} + i(b_1 \pm b_2) \\ e^{i\theta} \pm e^{2i\theta} + i(b_1 \pm b_2) & 1 \pm e^{3i\theta} + i(\chi \pm b_3) \end{bmatrix}.$$
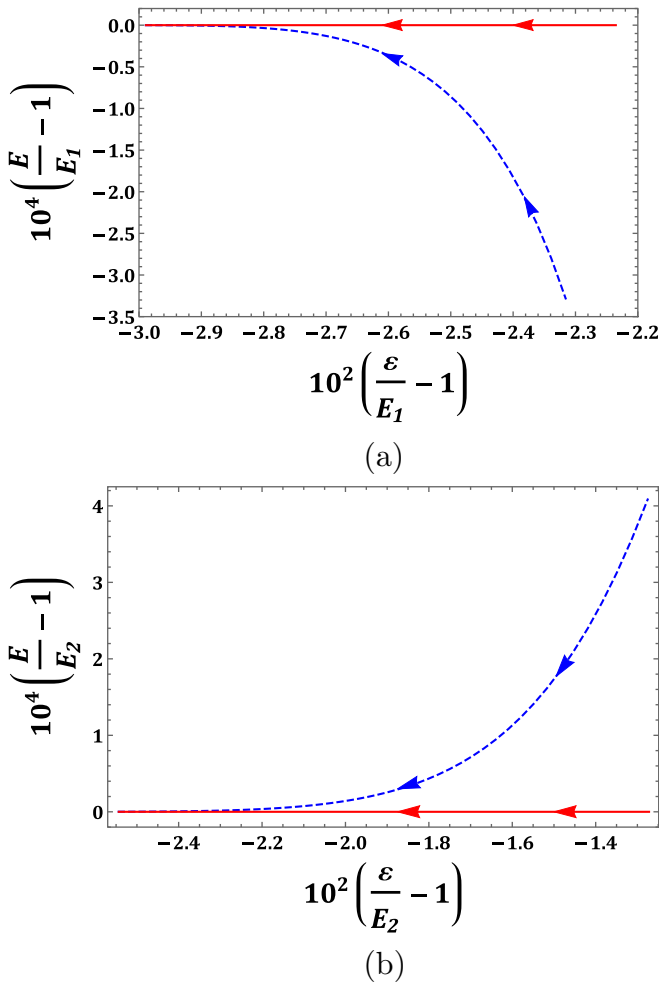
$$(64)$$

(a)

(b)

FIG. 5. Behavior of the bound-state energies E in the vicinity of the resonant values $E_1(d)$ (upper panel) and $E_2(d)$ (lower panel) for $n = 3$, as a function of ε. In both panels, the trajectories for symmetric (dashed blue lines) and antisymmetric states (solid red lines) are shown with the arrows pointing toward increasing emitter separation d. Notice that the antisymmetric bound state corresponds in both cases to the resonant energy, while the energy of the symmetric state approaches the resonant value as d increases (as ε decreases).

If the cut contributions are neglected, $\boldsymbol{b} = \boldsymbol{0}$, then the singularity conditions yield $\theta = \nu\pi$ and $\chi = 0$ as in (39), and two complementary pictures emerge according to the parity of ν. For even ν, the three-dimensional subspace corresponding to the eigenvalue $E_\nu(d)$ is spanned by the whole antisymmetric sector and by the symmetric state with

$$a_1 = -a_2 = -a_3 = a_4. \tag{65}$$

For odd ν, the eigenspace of $E_\nu(d)$ is still three dimensional, spanned by the whole symmetric sector and by the antisymmetric state with

$$a_1 = a_2 = -a_3 = -a_4. \tag{66}$$

When the $b_{j>0}$ terms are included, there are still eigenstates with resonant energy $E_\nu(d)$ in the antisymmetric sector for even ν and in the symmetric sector for odd ν. In the former case, such states occur when the parameters $(\varepsilon, d, \gamma, m)$
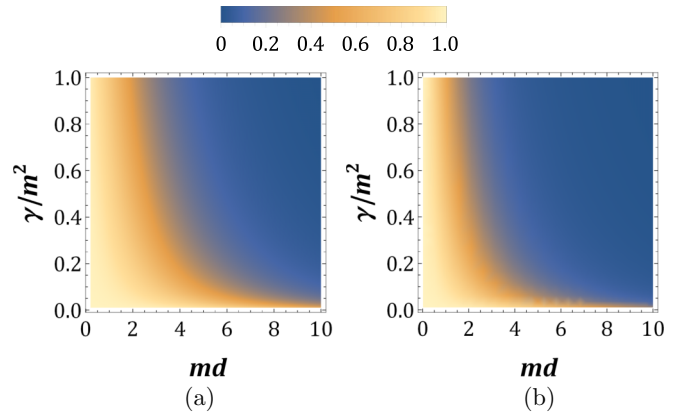

(a) (b)

FIG. 6. Total atomic excitation probability $p = \boldsymbol{a}^\dagger \boldsymbol{a}$, for $n = 3$ emitters, for the symmetric (left panel) and antisymmetric bound states with energy close to $E_1(d)$. In panel (a), $a_3 = a_1$ and $a_2/a_1 \simeq 2$; in panel (b), $a_3 = -a_1$ and $a_2 = 0$. The color scale is reported above the plots. We used the expressions (62)–(63).

satisfy

$$[\chi(E_\nu) - b_1(E_\nu)][\chi(E_\nu) - b_3(E_\nu)] = [b_1(E_\nu) - b_2(E_\nu)]^2, \tag{67}$$

which yields the two antisymmetric eigenstates characterized, at the lowest order in b_j, by the amplitudes

$$a_1 = -\frac{1 \pm \sqrt{5}}{2} a_2 = \frac{1 \pm \sqrt{5}}{2} a_3 = -a_4 \tag{68}$$

and the atomic excitation probabilities

$$p_\nu^{(4)}(\alpha) \simeq \left[1 + \alpha \frac{\gamma d E_\nu}{E_\nu^2 - m^2} + \frac{\gamma}{\pi(E_\nu + m)} \right]^{-1}, \tag{69}$$

where the value of α is found to be

$$\alpha = \frac{9 \pm \sqrt{5}}{5 \pm \sqrt{5}}. \tag{70}$$

In the case of odd ν, if the parameters satisfy

$$[\chi(E_\nu) + b_1(E_\nu)][\chi(E_\nu) + b_3(E_\nu)] = [b_1(E_\nu) + b_2(E_\nu)]^2, \tag{71}$$

then one finds symmetric eigenstates with $E = E_\nu(d)$, amplitudes

$$a_1 = -\frac{1 \pm \sqrt{5}}{2} a_2 = -\frac{1 \pm \sqrt{5}}{2} a_3 = a_4, \tag{72}$$

and atomic excitation probabilities $p_\nu^{(4)}(\alpha)$ in (69), with

$$\alpha = \frac{13 \pm \sqrt{5}}{5 \pm \sqrt{5}}. \tag{73}$$

These states are represented in Figs. 3(c)–3(f) for some values of the parameters d and γ. The atomic probabilities of the four classes of eigenstates defined by Eqs. (68)–(72) are shown in Fig. 7.

The states defined by the amplitudes (65) and (66) persist as eigenstates even after the introduction of the cut integration terms, $\boldsymbol{b} \neq \boldsymbol{0}$. However, their energies and the ratios between local amplitudes are shifted by a quantity $O(e^{-md})$
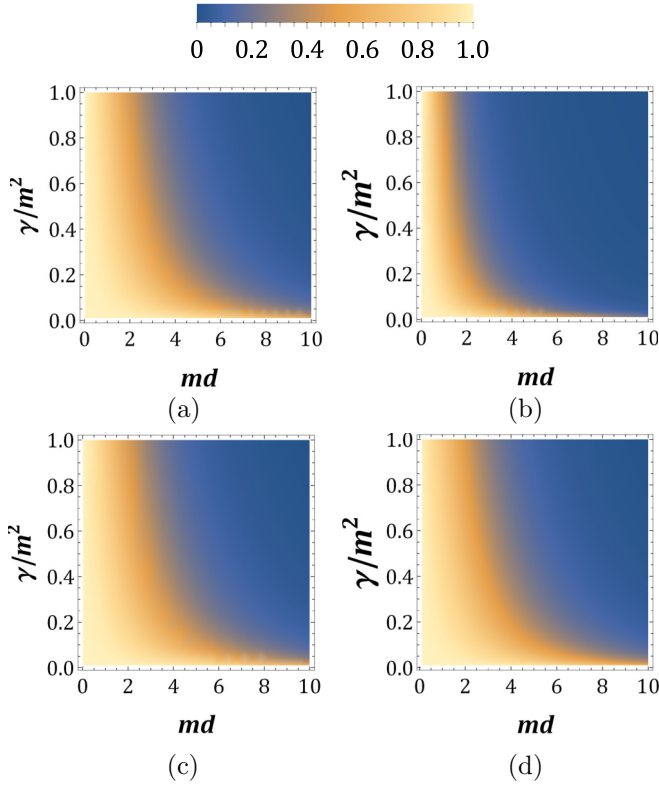
FIG. 7. Total atomic excitation probability $p = \boldsymbol{a}^{\dagger}\boldsymbol{a}$, when $n = 4$, for the eigenstates defined by Eqs. (68)–(72), characterized by a resonant energy $E_1(d)$ (upper panels), and for the two stable states (66) and (75), with $E < E_1(d)$ (lower panels). In panel (a) $a_1 = a_4$, $a_2 = a_3$, and $a_1/a_2 \simeq -(1 + \sqrt{5})/2$; in panel (b), $a_1 = a_4$, $a_2 = a_3$, and $a_1/a_2 \simeq -(1 - \sqrt{5})/2$; in panel (c), $a_1 = -a_4$, $a_2 = -a_3$, and $\frac{a_1}{a_2} \simeq 1$; in panel (d), $a_1 = a_4$, $a_2 = a_3$, and $a_1/a_2 \simeq 0.33$. The color scale is reported above the plots.

with respect to $E_\nu(d)$ and to the values in Eqs. (65) and (66), respectively. Specifically, at a fixed distance d, the antisymmetric state with amplitudes connected by continuity to (66) is characterized by an eigenvalue $E < E_\nu(d)$, slightly smaller than the resonant value. The total atomic probabilities corresponding to states in this class is given by $p_\nu^{(4)}(\alpha)$ in (69), with

$$\alpha = 1, \tag{74}$$

with even ν, for the symmetric state, and odd ν, for the antisymmetric one.

A numerical analysis of the determinant of the matrices (64) reveals the existence of a new class of nondegenerate bound states, characterized, in the distance range $2 \lesssim md \lesssim 6$, by the amplitudes

$$a_1 = a_4, \quad a_2 = a_3 \simeq 3a_1, \tag{75}$$

with energy close to $E_\nu(d)$ for odd ν, and

$$a_1 = -a_4, \quad a_2 = -a_3 \simeq -3a_1, \tag{76}$$

with energy close to $E_\nu(d)$ for even ν. The energy of such states is shifted with respect to the resonant values. In particular, one of the symmetric states (75) is characterized by an eigenvalue slightly smaller than $E_1(d)$, which makes it the
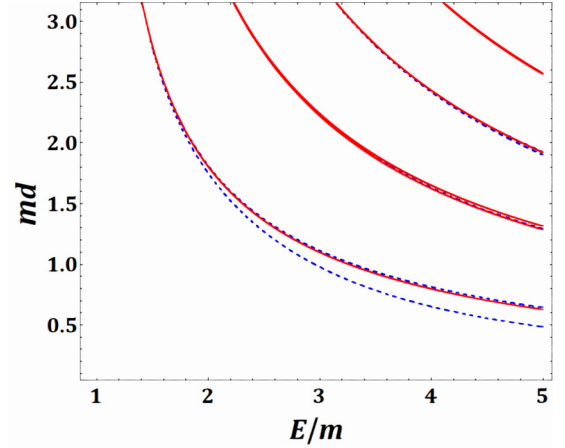

FIG. 8. Spectral lines in the (E, d) plane for a system of $n = 4$ equally spaced emitters. The solid (red) lines correspond to antisymmetric configurations, while dashed (blue) lines to symmetric ones. As in the $n = 3$ case, the approximation of the resonant values in Eq. (41) becomes more and more effective for larger values of the distance. For $md \lesssim 2$, the difference between the eigenvalues of the lowest-energy symmetric and antisymmetric states becomes appreciable, with a symmetric state characterized by the amplitudes (75) being related to the lowest eigenvalue at a fixed md.

lowest-energy bound state in the continuum for a system of $n = 4$ emitters at a fixed spacing d, as can be observed in Fig. 8. The states (75) and (76) are characterized by an emitter excitation probability $p_\nu^{(4)}(\alpha)$ in (69), with

$$\alpha = \tfrac{3}{5}. \tag{77}$$

The behavior of the lowest-energy bound states in the continuum is shown in detail in Fig. 9.

V. HIGH-ENERGY EIGENSTATES

Condition (18), which determines the eigenvalues of the system, is a complicated equation in E, featuring the functions $\theta(E)$, $\chi(E)$, and $\boldsymbol{b}(E)$. In the previous section, we have analyzed the solutions that can be connected by continuity to the resonant energies (41) in the limit $e^{-md} \to 0$. However, the nonpolynomial character of Eq. (18) can generally gives rise to new solutions at finite d, which are unrelated to the resonant eigenvalues and eigenspaces. In particular, this phenomenon is facilitated for very small md, when the magnitude of all the $b_{j>0}$ is relevant and comparable to that of b_0.

Figures 10 and 11 display general features of such nonperturbative states, for $n = 3$ and $n = 4$ emitters, respectively. These features are confirmed for higher n. At a sufficiently high value of the distance, all the eigenvalues are connected by continuity to the resonant energies $E_\nu(d)$, with $\nu \in \mathbb{Z}_+$. When distance decreases, additional eigenvalues start appearing in the (E, d) plane, between $E_\nu(d)$ and $E_{\nu+1}(d)$, immediately branching in two distinct eigenvalues, whose energy increases when distance is further decreased. The observed processes of pair formation in the cases $n = 3, 4$ occur roughly at the same value of d. To quantify the range in which the phenomenon occurs we define the critical distance $d_c^{(n)}$ as the value which marks the appearance of the first eigenstate of this class
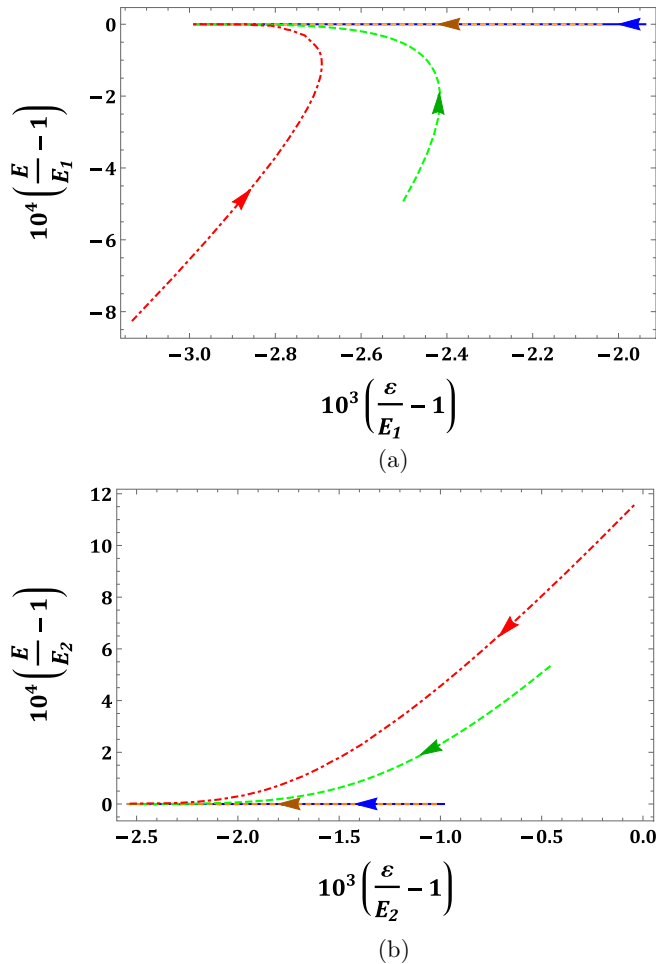
(a)

(b)

FIG. 9. Behavior of the bound-state energies E in the vicinity of the resonant values $E_1(d)$ (upper panel) and $E_2(d)$ (lower panel) for $n = 4$ as a function of ε. The two variables have been accordingly rescaled to show the most relevant details in the two panels. The solid (blue) and dotted (brown) lines, that are in practice superposed, are relative to the states defined by the amplitudes (72), the dashed (green) lines describe the energy of the states (66) in the upper panel and (65) in the lower panel, while the dot-dashed (red) lines coincide with the energy of the configurations (75) in the upper panel and (76) in the lower panel. In all curves, the arrows point toward increasing distance d. While the energy of states (72) are equal to the closest resonant value for all spacings, the eigenvalues related to the other states approach the resonant energies as d increases.

between $E_1(d)$ and $E_2(d)$. We obtain the values $md_c = 0.063$ for $n = 3$ emitters and $md_c = 0.052$ for $n = 4$ emitters. Notice that no state of this kind is observed with energy below $E_1(d)$. The value of energy E_c corresponding to the critical distance is $E_c/m \simeq 79$ for $n = 3$ and $E_c/m \simeq 101$ for $n = 4$. Thus, independently of the values of the parameters ε and γ, the energy of such states exceeds the mass m by at least two orders of magnitude, an energy range in which the validity of our model, at least in a waveguide QED context, is far from being ensured. However, as one can observe from Table I, the critical energy decreases to an order 10 for larger systems.

The nonperturbative eigenvalues always correspond to symmetric eigenstates, with a photon half-wavelength that is far from multiple integers of the interatomic spacing, as can
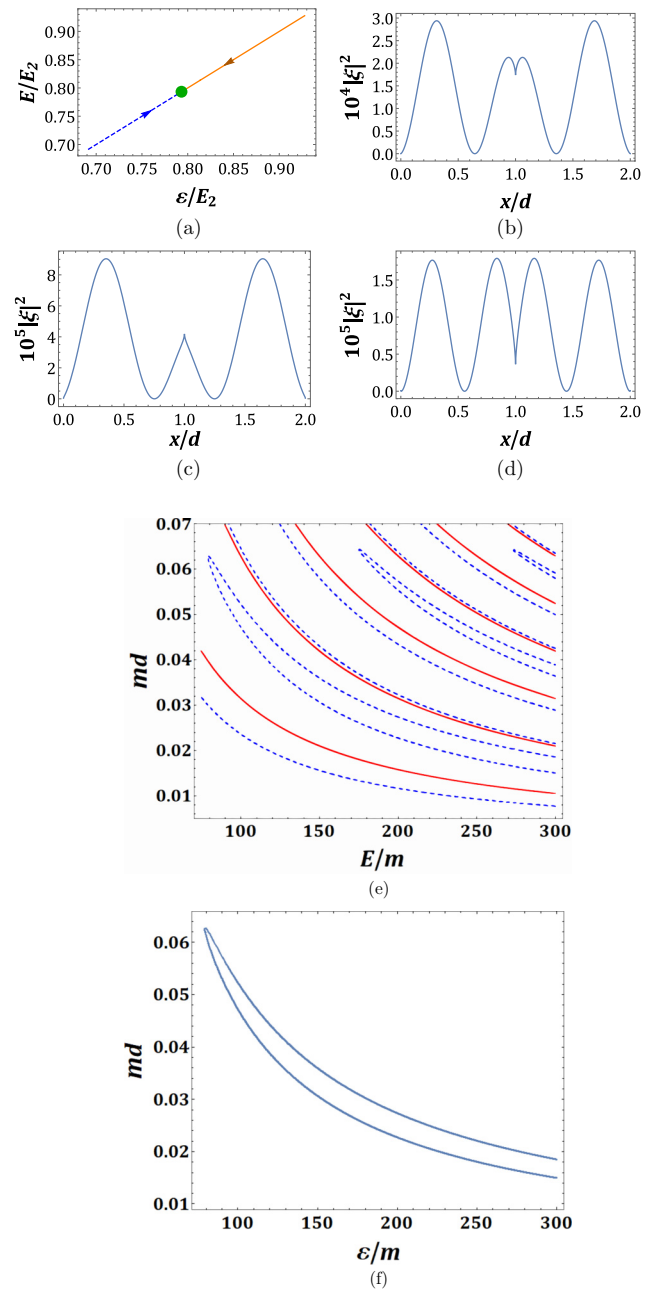

FIG. 10. Nonperturbative high-energy eigenstates for $n = 3$. (a) Energy trajectory of the pair of eigenstates with energy between E_1 and E_2 in the (ε, E) plane (in units of E_2), with the arrows pointing toward increasing values of md. At $md = md_c = 0.063$, the two eigenvalues coalesce and disappear. (b) Field probability density $|\xi(x)|^2$ corresponding to the critical case. [(c) and (d)] Field probability density $|\xi(x)|^2$ for the pair of bound states corresponding to the (very) small distance $md = 10^{-2}$. (e) Spectral lines in the (E, d) plane, with solid (red) lines representing antisymmetric states and dashed (blue) lines representing the symmetric ones; three branching points of eigenvalue pairs are visible. (f) Emitter excitation energies of the lowest-energy nonperturbative eigenstate pair as a function of d for $\gamma/m^2 = 10^{-2}$.

be observed in both Figs. 10 and 11. From the expression (10) one infers that, in such high-energy states, the field wave function is suppressed and the single excitation is almost
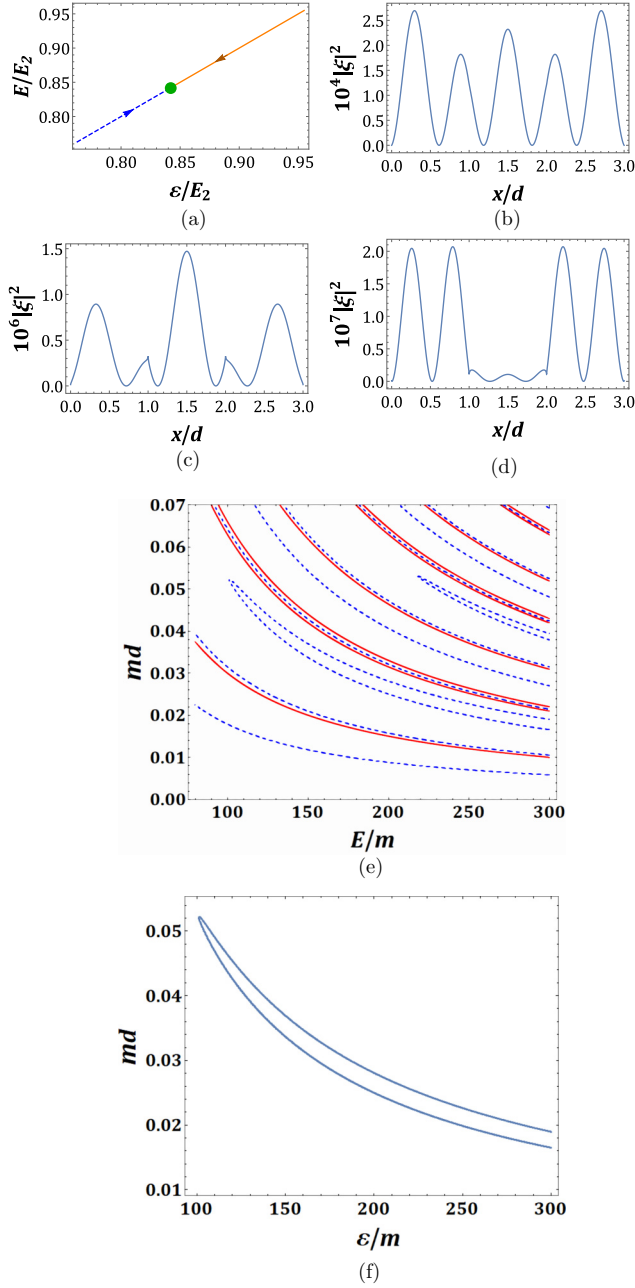
TABLE I. Critical values of the distance d_c at which the non-perturbative eigenvalue pair between the resonant energies E_1 and E_2 appears, and corresponding energy E_c, for arrays with different number of equally spaced emitters.

n	4	6	8	10	12
$m\,d_c$	0.05	0.18	0.26	0.30	0.33
E_c/m	101	28	20	16	15

VI. CONCLUSIONS

We have studied the existence and main features of bound states in the continuum for a multiemitter system in a one-dimensional configuration. We have found that, remarkably, finite-spacing effects can lift degeneracies, affecting eigenstates, eigenvalues and the physical model that features specific bound states. Future research will be devoted to the study of degeneracy lifting and the ensuing collective effects in systems with a large number of emitters.

APPENDIX A: GENERAL PROPERTIES OF THE EIGENVALUE EQUATION

The method used to characterize resonant bound states for a system of n emitters in the case of general n is based on the decomposition (37) in decoupled parity sectors. In Sec. IV B, we proved that, neglecting the $b_{j>0}$ terms, the eigenvalue equation reduces to $\chi(E) = 0$, yielding $(n-1)$-times degenerate eigenvalues $E_\nu(d)$, with $\nu \in \mathbb{Z}_+$, corresponding to eigenvectors whose atomic excitation amplitudes are constrained by (43) or (44) according to the sign $(-1)^\nu$. Here, we prove that the resonant energies $E_\nu(d)$ persist as exact eigenvalues even after the introduction of cut integration terms, for some value of the excitation energy ε.

The reduction to a block-diagonal form provided by the transformations (32) and (33) enables one to recast the eigenvalue equation into the decoupled problems

$$\det\left(A_n^\pm[\theta(E), \chi(E), \boldsymbol{b}(E)]\right) = 0. \tag{A1}$$

For definiteness, let us first consider the case of even $n = 2h$. Let us introduce for convenience the quantities

$$\beta_j^\nu = \begin{cases} \chi[E_\nu(d)] & \text{if } j = 0 \\ b_j[E_\nu(d)] & \text{if } j > 0 \end{cases} \tag{A2}$$

and the real and symmetric matrices

$$\mathcal{A}_q^\nu = \begin{pmatrix} \beta_0^\nu & \beta_1^\nu & \beta_2^\nu & \cdots & \beta_{q-1}^\nu \\ \beta_1^\nu & \beta_0^\nu & \beta_1^\nu & \cdots & \beta_{q-2}^\nu \\ \beta_2^\nu & \beta_1^\nu & \beta_0^\nu & \cdots & \beta_{q-3}^\nu \\ \vdots & \vdots & \vdots & \ddots & \vdots \\ \beta_{q-1}^\nu & \beta_{q-2}^\nu & \beta_{q-3}^\nu & \cdots & \beta_0^\nu \end{pmatrix}, \tag{A3}$$

FIG. 11. Nonperturbative high-energy eigenstates for $n = 4$. (a) Energy trajectory of the pair of eigenstates with energy between E_1 and E_2 in the (E, ε) plane (in units of E_2), with the arrows pointing toward increasing values of md. At $md = md_c = 0.052$, the two eigenvalues coalesce and disappear. (b) Field probability density $|\xi(x)|^2$ corresponding to the critical case. [(c) and (d)] Field probability density $|\xi(x)|^2$ for the pair of bound states corresponding to the (very) small $md = 10^{-4}$. (e) Spectral lines in the (E, d) plane, with solid (red) lines representing antisymmetric states and dashed (blue) lines representing the symmetric ones; three branching points of eigenvalue pairs are visible. (f) Emitter excitation energies of the lowest-energy nonperturbative eigenstate pair as a function of d for $\gamma/m^2 = 10^{-2}$.

entirely shared by the emitters. Finally, for $n > 4$, we have found the existence of more than one pair of nonperturbative eigenstates between E_ν and $E_{\nu+1}$.

$$\mathcal{B}^{v}_{q,p} = \begin{pmatrix} \beta^{v}_{q} & \beta^{v}_{q-1} & \beta^{v}_{q-2} & \cdots & \beta^{v}_{q-p} \\ \beta^{v}_{q-1} & \beta^{v}_{q-2} & \beta^{v}_{q-3} & \cdots & \beta^{v}_{q-p-1} \\ \beta^{v}_{q-2} & \beta^{v}_{q-3} & \beta^{v}_{q-4} & \cdots & \beta^{v}_{q-p-2} \\ \vdots & \vdots & \vdots & \ddots & \vdots \\ \beta^{v}_{q-p} & \beta^{v}_{q-p-1} & \beta^{v}_{q-p-2} & \cdots & \beta^{v}_{q-2p} \end{pmatrix}, (A4)$$

and $\mathcal{C}^{\pm}_{q}$ as the $q \times q$ matrix characterized by the elements

$$[\mathcal{C}^{\pm}_{q}]_{j\ell} = (\pm 1)^{j+\ell}. \tag{A5}$$

If v is even, then

$$-iA^{-}_{2h}(v\pi, \chi[E_{v}(d)], \boldsymbol{b}[E_{v}(d)]) = \mathcal{A}^{v}_{h} - \mathcal{B}^{v}_{2h-1,h-1} \quad (A6)$$

and

$$-iA^{+}_{2h}(v\pi, \chi[E_{v}(d)], \boldsymbol{b}[E_{v}(d)]) = \mathcal{A}^{v}_{h} + \mathcal{B}^{v}_{2h-1,h-1} - 2i\mathcal{C}^{+}_{h}, \tag{A7}$$

while, for odd v,

$$-iA^{+}_{2h}(v\pi, \chi[E_{v}(d)], \boldsymbol{b}[E_{v}(d)]) = \mathcal{A}^{v}_{h} + \mathcal{B}^{v}_{2h-1,h-1} \quad (A8)$$

and

$$-iA^{-}_{2h}(v\pi, \chi[E_{v}(d)], \boldsymbol{b}[E_{v}(d)]) = \mathcal{A}^{v}_{h} + \mathcal{B}^{v}_{2h-1,h-1} - 2i\mathcal{C}^{-}_{h}. \tag{A9}$$

Fixing $E = E_{v}(d)$ and considering the expression of $\chi(E)$, Eq. (A1) can be generally recast in the form

$$\det(\mathcal{M} - \varepsilon\mathbb{1}) = 0, \tag{A10}$$

implying that $E_{v}(d)$ is an eigenvalue of the system if and only if ε is the *real* eigenvalue of some matrix $\mathcal{M}$. From the expressions (A6)–(A8), one can notice that, in the antisymmetric sector for even v and in the symmetric sector for odd v, the matrix $\mathcal{M}$ is Hermitian, entailing the existence of n values of ε, real and *generally distinct*, corresponding to physical systems in which a bound state with energy $E_{v}(d)$ is present. Those values of ε collapse to a single degenerate value in the $e^{-md} \to 0$ limit. In the cases (A7)–(A9), instead, $\mathcal{M}$ is not Hermitian, its the eigenvalues are generally no longer real, and the bound-state energies displace from the resonant values.

The case of odd $n = 2h + 1$ is slightly different. There, for all resonance orders v, in the antisymmetric sector

$$-iA^{-}_{2h+1}(v\pi, \chi[E_{v}(d)], \boldsymbol{b}[E_{v}(d)]) = \mathcal{A}^{v}_{h} - \mathcal{B}^{v}_{2h,h-1}, \quad (A11)$$

leading to a condition (A10) with a Hermitian $\mathcal{M}$, which implies that all the $E_{v}(d)$ are eigenvalues corresponding to antisymmetric bound states for generally different physical systems. On the other hand, the matrix $\mathcal{M}$ corresponding to all resonances in the symmetric sector is never Hermitian, since it features an imaginary and symmetric contribution proportional to $\mathcal{C}^{\pm}_{h+1}$.

APPENDIX B: UNSTABLE STATES

The resolvent formalism, employed in the main text to evaluate the existence and properties of bound states, also provides information on the lifetime of unstable states. The step required to perform this kind of analysis in the analytic continuation of the self-energy to the second Riemann sheet

$$\Sigma^{(II)}_{j\ell}(z) = \Sigma_{j\ell}(z) - \frac{2i\gamma}{\sqrt{z^2 - m^2}} \cos[|j - \ell|\theta(z)], \tag{B1}$$

where z is a complex energy. The lifetimes of unstable states are determined by the solutions $z_p = E_p - i\gamma_p/2$ of the equation

$$\det\left\{[G^{(II)}]^{-1}\left(E_p - i\frac{\gamma_p}{2}\right)\right\} = 0 \quad \text{with } \gamma_p > 0, \tag{B2}$$

with

$$[G^{(II)}]^{-1}(z) = (z - \varepsilon)\mathbb{1} - \Sigma^{(II)}(z). \tag{B3}$$

We are now going to consider the properties of the complex poles of the propagator.

1. $n = 3$ emitters

The block-diagonalization procedure applied to a system of three emitters implies the singularity conditions:

$$\chi(z) = -\frac{i}{2}[2 + e^{-2i\theta(z)}] - \frac{b_2(z)}{2} \pm \frac{1}{2}\sqrt{f_3[\theta(z), \boldsymbol{b}(z)]}, \tag{B4}$$

for symmetric states, and

$$\chi(z) = b_2(z) - i[1 - e^{-2i\theta(z)}], \tag{B5}$$

for antisymmetric states, with

$$f_3(\theta, \boldsymbol{b}) = 8b_1^2 + b_2^2 + 16ib_1e^{-i\theta} - 8e^{-2i\theta} + 2ib_2e^{-2i\theta} - e^{-4i\theta}. \tag{B6}$$
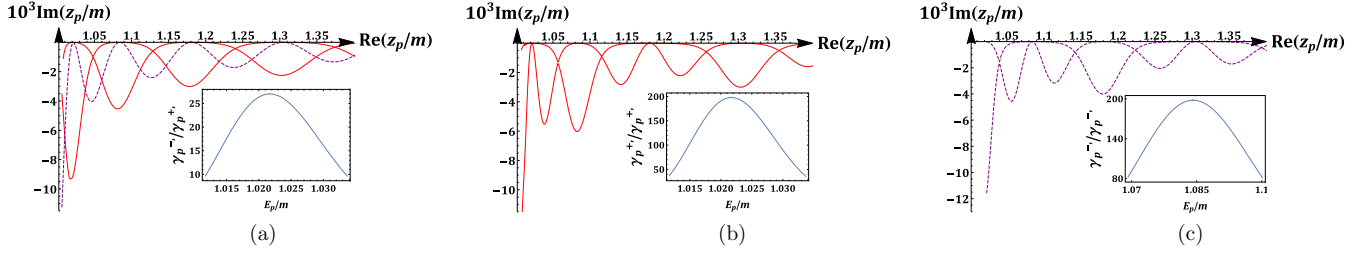
FIG. 12. Pole trajectories in the lower half-plane of complex energy for $n = 3$ (a) and $n = 4$ [(b) and (c)]. The parameters are set to $md = 15$ and $\gamma/m^2 = 2\pi \times 10^{-4}$, while ε varies between m and $1.4m$. Solid (red) lines are associated with symmetric eigenstates, while dashed (purple) lines refer to antisymmetric states. In the insets, we report the ratios between the first derivatives $d\mathrm{Im}(z_p)/d\mathrm{Re}(z_p)$ related to two different curves, both approaching the real axis (i.e., corresponding to a stable bound state) at the same point, corresponding to the lowest-energy resonance in the plots. Notice that, close to the resonance points, the imaginary parts of the unstable poles scale linearly with n.

Introducing the functions $R_3(\theta, \boldsymbol{b}) = \mathrm{Re}[f_3(\theta, \boldsymbol{b})]$, $S_3(\theta, \boldsymbol{b}) = \mathrm{Im}[f_3(\theta, \boldsymbol{b})]$, the real and imaginary part of roots of the complex poles for the two blocks read

$$E_p^+ \approx \varepsilon + \frac{\gamma}{2\bar{k}(E_p^+)} \left\{ 2b_0(E_p^+) + b_2(E_p^+) + \sin\left[2\theta(E_p^+)\right] \mp \sqrt{\frac{R_3(\theta, \mathbf{b}) + \sqrt{R_3^2(\theta, \mathbf{b}) + S_3^2(\theta, \mathbf{b})}}{2}} \right\} \tag{B7}$$

$$\frac{\gamma_p^+}{2} \approx \frac{\gamma}{2\bar{k}(E_p^+)} \left\{ 2 + \cos\left[2\theta(E_p^+)\right] \pm \sqrt{\frac{-R_3(\theta, \mathbf{b}) + \sqrt{R_3^2(\theta, \mathbf{b}) + S_3^2(\theta, \mathbf{b})}}{2}} \right\}, \tag{B8}$$

$$E_p^- \approx \varepsilon + \frac{\gamma}{\bar{k}(E_p^-)} \{ b_0(E_p^-) + b_2(E_p^-) + \sin\left[2\theta(E_p^-)\right] \}, \tag{B9}$$

$$\frac{\gamma_p^-}{2} \approx \frac{\gamma}{\bar{k}(E_p^-)} \{ 1 - \cos\left[2\theta(E_p^-)\right] \}, \tag{B10}$$

with $\bar{k}(E) = \sqrt{E^2 - m^2}$. The behavior of the complex poles of the propagator for $n = 3$ is reported in panel (a) of Fig. 12.

2. $n = 4$ emitters

The singularity condition for the symmetric and antisymmetric blocks in the $n = 4$ system read

$$\chi(z) = -\frac{i}{2}[2 + e^{-i\theta(z)} + e^{-3i\theta(z)}] - \frac{b_1(z) + b_3(z)}{2} \pm \frac{1}{2}\sqrt{f_4^+[\theta(z), \boldsymbol{b}(z)]}, \tag{B11}$$

$$\chi(z) = \frac{i}{2}[-2 + e^{-i\theta(z)} + e^{-3i\theta(z)}] + \frac{b_1(z) + b_3(z)}{2} \pm \frac{1}{2}\sqrt{f_4^-[\theta(z), \boldsymbol{b}(z)]}, \tag{B12}$$

respectively, with

$$f_4^+(\theta, \boldsymbol{b}) = 4(b_1 + b_2)^2 + (b_1 - b_3)^2 + i(10b_1 + 8b_2 - 2b_3)e^{-i\theta}$$
$$+ i(5i + 8b_1 + 8b_2)e^{-2i\theta} + i(8i - 2b_1 + 2b_3)e^{-3i\theta} - 2e^{-4i\theta} - e^{-6i\theta}, \tag{B13}$$

$$f_4^-(\theta, \boldsymbol{b}) = 4(b_1 - b_2)^2 + (b_1 - b_3)^2 + i(10b_1 - 8b_2 - 2b_3)e^{-i\theta}$$
$$+ i(5i - 8b_1 + 8b_2)e^{-2i\theta} - i(8i + 2b_1 - 2b_3)e^{-3i\theta} - 2e^{-4i\theta} - e^{-6i\theta}, \tag{B14}$$

where we have defined $R_4^\pm(\theta, \boldsymbol{b}) = \mathrm{Re}[f_4^\pm(\theta, \boldsymbol{b})]$, $S_4^\pm(\theta, \boldsymbol{b}) = \mathrm{Im}[f_4^\pm(\theta, \boldsymbol{b})]$. In this way approximate decoupled solutions are

$$E_p^+ \approx \varepsilon + \frac{\gamma}{2\bar{k}(E_p^+)} \left[2b_0(E_p^+) + b_1(E_p^+) + b_3(E_p^+) + \sin(\theta) + \sin(3\theta) \mp \sqrt{\frac{R_4^+(\theta, \boldsymbol{b}) + \sqrt{R_4^{+2}(\theta, \boldsymbol{b}) + S_4^{+2}(\theta, \boldsymbol{b})}}{2}} \right], \tag{B15}$$

$$\frac{\gamma_p^+}{2} \approx \frac{\gamma}{2\bar{k}(E_p^+)} \left[2 + \cos(\theta) + \cos(3\theta) \pm \sqrt{\frac{-R_4^+(\theta, \boldsymbol{b}) + \sqrt{R_4^{+2}(\theta, \boldsymbol{b}) + S_4^{+2}(\theta, \boldsymbol{b})}}{2}} \right], \tag{B16}$$
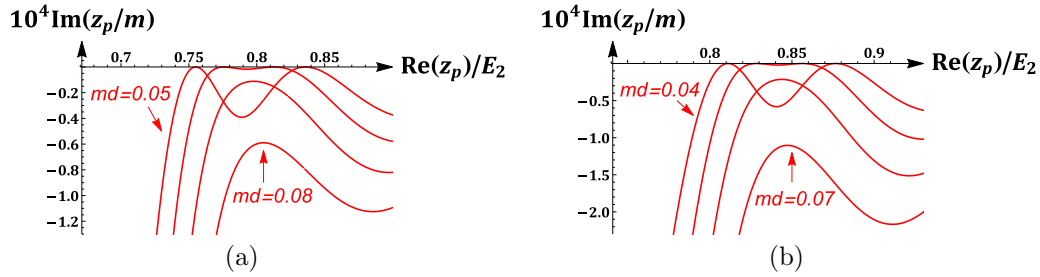
FIG. 13. Trajectories of poles with real part between $E_1(d)$ and $E_2(d)$ in the complex lower half-plane, for different values of md in a system of $n = 3$ (left) and $n = 4$ (right). The emergence of nonperturbative eigenstates is related to the pole trajectory touching the real axis at a critical distance. Below the critical distance, the trajectories are tangent to the real axis in two points.

$$E_p^- \approx \varepsilon + \frac{\gamma}{2\bar{k}(E_p^-)} \left[b_0(E_p^-) - b_1(E_p^-) - b_3(E_p^-) - \sin(\theta) - \sin(3\theta) \mp \sqrt{\frac{R_4^-(\theta, \boldsymbol{b}) + \sqrt{R_4^{-2}(\theta, \boldsymbol{b}) + S_4^{-2}(\theta, \boldsymbol{b})}}{2}} \right], \quad \text{(B17)}$$

$$\frac{\gamma_p^-}{2} \approx \frac{\gamma}{2\bar{k}(E_p^-)} \left[2 - \cos(\theta) - \cos(3\theta) \pm \sqrt{\frac{-R_4^-(\theta, \boldsymbol{b}) + \sqrt{R_4^{-2}(\theta, \boldsymbol{b}) + S_4^{-2}(\theta, \boldsymbol{b})}}{2}} \right], \quad \text{(B18)}$$

with $\bar{k}(E) = \sqrt{E^2 - m^2}$. The behavior of the complex poles of the propagator for $n = 4$ in the symmetric and antisymmetric sectors is shown in Figs. 12(b) and 12(c).

We finally comment on the phenomenon of emergence of nonperturbative eigenstates for small values of md. Such poles appear when one of the complex poles with negative imaginary part in the second Riemann sheet approaches the real axis (see Fig. 13). Due to the analytic properties of the resolvent, there is a symmetric pole of the analytic continuation

$$\Sigma_{j\ell}^{(\mathrm{III})}(z) = \Sigma_{j\ell}(z) + \frac{2i\gamma}{\sqrt{z^2 - m^2}} \cos[|j - \ell|\theta(z)] \quad \text{(B19)}$$

in the upper half-plane. At $d = d_c$ the two poles collide and coalesce at a point of the real axis. By further decreasing the spacing d, the two poles split up along the real axis and increase their energy difference.

[1] D. Roy, C. M. Wilson, and O. Firstenberg, Colloquium: Strongly interacting photons in one-dimensional continuum, Rev. Mod. Phys. **89**, 021001 (2017).

[2] E. Vetsch, D. Reitz, G. Sague, R. Schmidt, S. T. Dawkins, and A. Rauschenbeutel, Optical Interface Created by Laser-Cooled Atoms Trapped in the Evanescent Field Surrounding an Optical Nanofiber, Phys. Rev. Lett. **104**, 203603 (2010).

[3] M. Bajcsy, S. Hofferberth, V. Balic, T. Peyronel, M. Hafezi, A. S. Zibrov, V. Vuletic, and M. D. Lukin, Efficient All-Optical Switching Using Slow Light within a Hollow Fiber, Phys. Rev. Lett. **102**, 203902 (2009).

[4] U. Dorner and P. Zoller, Laser-driven atoms in half-cavities, Phys. Rev. A **66**, 023816 (2002).

[5] G. Zumofen, N. M. Mojarad, V. Sandoghdar, and M. Agio, Perfect Reflection of Light by an Oscillating Dipole, Phys. Rev. Lett. **101**, 180404 (2008).

[6] N. Lindlein, R. Maiwald, H. Konermann, M. Sondermann, U. Peschel, and G. Leuchs, A new 4π geometry optimized for focusing on an atom with a dipole-like radiation pattern, Laser Phys. **17**, 927 (2007).

[7] P. Lodahl, S. Mahmoodian, and S. Stobbe, Interfacing single photons and single quantum dots with photonic nanostructures, Rev. Mod. Phys. **87**, 347 (2015).

[8] A. Wallraff, D. I. Schuster, A. Blais, L. Frunzio, R.-S. Huang, J. Majer, S. Kumar, S. M. Girvin, and R. J. Schoelkopf, Strong coupling of a single photon to a superconducting qubit using circuit quantum electrodynamics, Nature **431**, 162 (2004).

[9] O. Astafiev, A. M. Zagoskin, A. A. Abdumalikov, Jr., Yu. A. Pashkin, T. Yamamoto, K. Inomata, Y. Nakamura, and J. S. Tsai, Resonance fluorescence of a single artificial atom, Science **327**, 840 (2010).

[10] I.-C. Hoi, A. F. Kockum, L. Tornberg, A. Pourkabirian, G. Johansson, P. Delsing, and C. M. Wilson, Probing the quantum vacuum with an artificial atom in front of a mirror, Nat. Phys. **11**, 1045 (2015).

[11] H. Dong, Z. R. Gong, H. Ian, L. Zhou, and C. P. Sun, Intrinsic cavity QED and emergent quasinormal modes for a single photon, Phys. Rev. A **79**, 063847 (2009).

[12] T. Tufarelli, F. Ciccarello, and M. S. Kim, Dynamics of spontaneous emission in a single-end photonic waveguide, Phys. Rev. A **87**, 013820 (2013).

[13] J.-T. Shen and S. Fan, Coherent Single Photon Transport in a One-Dimensional Waveguide Coupled with Superconducting Quantum Bits, Phys. Rev. Lett. **95**, 213001 (2005).

[14] A. Faraon, E. Waks, D. Englund, I. Fushman, and J. Vučković, Efficient photonic crystal cavity-waveguide couplers, Appl. Phys. Lett. **90**, 073102 (2007).

[15] B. Dayan, A. S. Parkins, Takao Aoki, E. P. Ostby, K. J. Vahala, and H. J. Kimble, A photon turnstile dynamically regulated by one atom, Science **319**, 1062 (2008).

[16] J. S. Douglas, H. Habibian, C.-L. Hung, A. V. Gorshkov, H. J. Kimble, D. E. Chang, Quantum many-body models with cold atoms coupled to photonic crystals, Nat. Photon. **9**, 326 (2015).

[17] A. Goban, C.-L. Hung, J. D. Hood, S.-P. Yu, J. A. Muniz, O. Painter, H. J. Kimble, Superradiance for Atoms Trapped along a Photonic Crystal Waveguide, Phys. Rev. Lett. **115**, 063601 (2015).

[18] A. González-Tudela, V. Paulisch, H. J. Kimble, and J. I. Cirac, Efficient Multiphoton Generation in Waveguide Quantum Electrodynamics, Phys. Rev. Lett. **118**, 213601 (2017).

[19] J. Bleuse, J. Claudon, M. Creasey, N. S. Malik, J.-M. Gérard, I. Maksymov, J.-P. Hugonin, and P. Lalanne, Inhibition, Enhancement, and Control of Spontaneous Emission in Photonic Nanowires, Phys. Rev. Lett. **106**, 103601 (2011).

[20] M. E. Reimer, G. Bulgarini, N. Akopian, M. Hocevar, M. B. Bavinck, M. A. Verheijen, E. P. A. M. Bakkers, L. P. Kouwenhoven, and V. Zwiller, Bright single-photon sources in bottom-up tailored nanowires, Nat. Commun. **3**, 737 (2012).

[21] T. Shi, D. E. Chang, and J. I. Cirac, Multiphoton-scattering theory and generalized master equations, Phys. Rev. A **92**, 053834 (2015).

[22] T. Shi, Y.-H. Wu, A. González-Tudela, and J. I. Cirac, Bound States in Boson Impurity Models, Phys. Rev. X **6**, 021027 (2016).

[23] E. Sanchez-Burillo, D. Zueco, L. Martin-Moreno, and J. J. Garcia-Ripoll, Dynamical signatures of bound states in waveguide QED, Phys. Rev. A **96**, 023831 (2017).

[24] F. Lombardo, F. Ciccarello, and G. M. Palma, Photon localization versus population trapping in a coupled-cavity array, Phys. Rev. A **89**, 053826 (2014).

[25] K. Lalumière, B. C. Sanders, A. F. van Loo, A. Fedorov, A. Wallraff, and A. Blais, Input-output theory for waveguide QED with an ensemble of inhomogeneous atoms, Phys. Rev. A **88**, 043806 (2013).

[26] D. Witthaut and A. S. Sørensen, Photon scattering by a three-level emitter in a one-dimensional waveguide, New J. Phys. **12**, 043052 (2010).

[27] A. Gonzalez-Tudela, D. Martin-Cano, E. Moreno, L. Martin-Moreno, C. Tejedor, and F. J. Garcia-Vidal, Entanglement of Two Qubits Mediated by One-Dimensional Plasmonic Waveguides, Phys. Rev. Lett. **106**, 020501 (2011).

[28] E. Shahmoon and G. Kurizki, Nonradiative interaction and entanglement between distant atoms, Phys. Rev. A **87**, 033831 (2013).

[29] P. Facchi, M. S. Kim, S. Pascazio, F. V. Pepe, D. Pomarico, and T. Tufarelli, Bound states and entanglement generation in waveguide quantum electrodynamics, Phys. Rev. A **94**, 043839 (2016).

[30] P. Facchi, S. Pascazio, F. V. Pepe, and K. Yuasa, Long-lived entanglement of two multilevel atoms in a waveguide, J. Phys. Commun. **2**, 035006 (2018).

[31] X. H. H. Zhang, and H. U. Baranger, Heralded Bell State of 1D Dissipative Qubits Using Classical Light, Phys. Rev. Lett. **122**, 140502 (2019).

[32] H. Zheng and H. U. Baranger, Persistent Quantum Beats and Long-Distance Entanglement from Waveguide-Mediated Interactions, Phys. Rev. Lett. **110**, 113601 (2013).

[33] C. Gonzalez-Ballestero, F. J. Garcia-Vidal, and E. Moreno, Non-Markovian effects in waveguide-mediated entanglement, New J. Phys. **15**, 073015 (2013).

[34] E. S. Redchenko and V. I. Yudson, Decay of metastable excited states of two qubits in a waveguide, Phys. Rev. A **90**, 063829 (2014).

[35] M. Laakso and M. Pletyukhov, Scattering of Two Photons from Two Distant Qubits: Exact Solution, Phys. Rev. Lett. **113**, 183601 (2014).

[36] H. Pichler, T. Ramos, A. J. Daley, P. Zoller, Quantum optics of chiral spin networks, Phys. Rev. A **91**, 042116 (2015).

[37] A. F. van Loo, A. Fedorov, K. Lalumière, B. C. Sanders, A. Blais, and A. Wallraff, Photon-mediated interactions between distant artificial atoms, Science **342**, 1494 (2013).

[38] A. Rosario Hamann, C. Müller, M. Jerger, M. Zanner, J. Combes, M. Pletyukhov, M. Weides, T. M. Stace, and A. Fedorov, Nonreciprocity Realized with Quantum Nonlinearity, Phys. Rev. Lett. **121**, 123601 (2018).

[39] G. Calajó, Yao-Lung L. Fang, H. U. Baranger, and F. Ciccarello, Exciting a Bound State in the Continuum Through Multiphoton Scattering Plus Delayed Quantum Feedback, Phys. Rev. Lett. **122**, 073601 (2019).

[40] V. I. Yudson, Dynamics of the integrable one-dimensional system "photons + two-level atoms," Phys. Lett. A **129**, 17 (1988).

[41] H. Pichler and P. Zoller, Photonic Circuits with Time Delays and Quantum Feedback, Phys. Rev. Lett. **116**, 093601 (2016).

[42] V. I. Yudson and P. Reineker, Multiphoton scattering in a one-dimensional waveguide with resonant atoms, Phys. Rev. A **78**, 052713 (2008).

[43] Y.-L. L. Fang and H. U. Baranger, Waveguide QED: Power spectra and correlations of two photons scattered off multiple distant qubits and a mirror, Phys. Rev. A **91**, 053845 (2015).

[44] T. S. Tsoi and C. K. Law, Quantum interference effects of a single photon interacting with an atomic chain inside a one-dimensional waveguide, Phys. Rev. A **78**, 063832 (2008).

[45] T. Ramos, B. Vermersch, P. Hauke, H. Pichler, and P. Zoller, Non-Markovian dynamics in chiral quantum networks with spins and photons, Phys. Rev. A **93**, 062104 (2016).

[46] M. Bello, G. Platero, J. I. Cirac, and A. González-Tudela, Unconventional quantum optics in topological waveguide QED, Sci. Adv. **5**, eaaw0297 (2019).

[47] H. Bernien, S. Schwartz, A. Keesling, H. Levine, A. Omran, H. Pichler, S. Choi, A. S. Zibrov, M. Endres, M. Greiner, V. Vuletić, and M. D. Lukin, Probing many-body dynamics on a 51-atom quantum simulator, Nature **551**, 579 (2017).

[48] Y. Dong, Y.-S. Lee, and K. S. Choi, Waveguide QED toolboxes for synthetic quantum matter with neutral atoms, arXiv:1712.02020 (2018).

[49] Y. Fang, H. Zheng, and H. Baranger, One-dimensional waveguide coupled to multiple qubits: photon-photon correlations, EPJ Quant. Technol. **1**, 3 (2014).

[50] X. Gu, A. F. Kockum, A. Miranowicz, Y.-X. Liu, and F. Nori, Microwave photonics with superconducting quantum circuits, Phys. Rep. **718**, 1 (2017).

[51] P. O. Guimond, H. Pichler, A. Rauschenbeutel, and P. Zoller, Chiral quantum optics with V-level atoms and coherent quantum feedback, Phys. Rev. A **94**, 033829 (2016).

[52] P. Lodahl, S. Mahmoodian, S. Stobbe, A. Rauschenbeutel, P. Schneeweiss, and J. Volz, Chiral quantum optics, Nature **541**, 473 (2017).

[53] V. Paulisch, H. Kimble, and A. González-Tudela, Universal quantum computation in waveguide QED using decoherence free subspaces, New J. Phys. **18**, 043041 (2016).

[54] T. Ramos, H. Pichler, A. J. Daley, and P. Zoller, Quantum Spin Dimers from Chiral Dissipation in Cold-Atom Chains, Phys. Rev. Lett. **113**, 237203 (2014).

[55] G. Calajo, F. Ciccarello, D. Chang, and P. Rabl, Atom-field dressed states in slow-light waveguide QED, Phys. Rev. A **93**, 033833 (2016).

[56] A. F. Kockum, Göran Johansson, and Franco Nori, Decoherence-Free Interaction between Giant Atoms in Waveguide Quantum Electrodynamics, Phys. Rev. Lett. **120**, 140404 (2018).

[57] F. Dinc, A. M. Brańczyk, and I. Ercan, Real-space time dynamics in waveguide QED: bound states and single-photon-pulse scattering, arXiv:1809.05164 (2018).

[58] R. H. Dicke, Coherence in spontaneous radiation processes, Phys. Rev. **93**, 99 (1954).

[59] M. Gross, S. Haroche, Superradiance: An essay on the theory of collective spontaneous emission, Phys. Rep. **93**, 301 (1982).

[60] M. O. Araújo, I. Krešić, R. Kaiser, and W. Guerin, Superradiance in a Large and Dilute Cloud of Cold Atoms in the Linear-Optics Regime, Phys. Rev. Lett. **117**, 073002 (2016).

[61] N. Cherroret, M. Hemmerling, V. Nador, J. T. M. Walraven, and R. Kaiser, Robust Coherent Transport of Light in Multi-Level Hot Atomic Vapors, Phys. Rev. Lett. **122**, 183203 (2019).

[62] C. W. Hsu, B. Zhen, A. D. Stone, J. D. Joannopoulos, and Marin Soljačić, Bound states in the continuum, Nat. Rev. Mater. **1**, 16048 (2016).

[63] C. Cohen-Tannoudji, J. Dupont-Roc, and G. Grynberg, *Atom-Photon Interactions: Basic Processes and Applications* (Wiley-VCH Verlag, Weinheim, 1998).

[64] P. Facchi, S. Pascazio, F. V. Pepe, and D. Pomarico, Correlated photon emission by two excited atoms in a waveguide, Phys. Rev. A **98**, 063823 (2018).